

h/e Oscillations in Interlayer Transport of Delafossites

Carsten Putzke^{1,2}, Maja D. Bachmann^{1,3}, Philippa McGuinness^{1,3}, Elina Zhakina¹, Takashi Oka^{1,4}, Roderich Moessner⁴, Markus König¹, Seunghyun Khim¹, Andrew P. Mackenzie^{1,3}, Philip J.W. Moll^{1,2}

¹Max Planck Institute for Chemical Physics of Solids, 01187 Dresden, Germany

²Institute of Material Science and Engineering, École Polytechnique Fédéral de Lausanne (EPFL), 1015 Lausanne, Switzerland

³School of Physics and Astronomy, University of St. Andrews, St. Andrews KY16 9SS, UK

⁴Max Planck Institute for the Physics of Complex Systems, 01187 Dresden, Germany

*To whom correspondence should be addressed: carsten.putzke@epfl.ch, philip.moll@epfl.ch

Transport of electrons in a metal is usually well captured by their particle-like aspects, while their wave-like nature is commonly unobservable. Microstructures can be carefully designed to shield the quantum phase of the electrons from decoherence due to external perturbations, for example mesoscopic metal rings resembling interferometers. Here we report a new type of phase coherent oscillation of the out-of-plane magnetoresistance in the layered delafossites PdCoO₂ and PtCoO₂. The oscillation period is equivalent to that determined by the magnetic flux quantum, h/e , threading an area defined by the atomic interlayer separation and the sample width. The phase of the electron wave function in these crystals appears remarkably robust over macroscopic length scales exceeding 5 μm and persisting up to elevated temperatures of 60K. While the microscopic origin of this effect remains to be clarified and challenges our understanding of interlayer transport in ultra-pure metals, the results suggest the feasibility of a novel class of magnetic field sensors of unprecedented atomic-scale spatial resolution.

Electrons in vacuum carry the characteristics of particles as well as waves, which is demonstrated in interference experiments directly probing the phase information¹. In metals the transport properties are usually well captured by the particle nature of the electron only, summarized in the semi-classical Boltzmann equation. The wave-like character is masked by the high density of electrons and their interaction with the ionic lattice, which leads to a loss of the phase information in bulk phenomena. With experimental effort, the sample can be fabricated on the mesoscopic length scale over which the phase of the electron is preserved, thus becoming observable in electronic transport. A well-known example is the Aharonov-Bohm effect in nanoscopic rings of gold^{2,3}, which presents a solid-state analog of the interference experiment by Davisson and Germer¹.

The main experimental observation we report here is an unexpected manifestation of phase coherence in the out-of-plane transport of the ultra-pure delafossites PdCoO₂ and PtCoO₂. These materials are composed of highly conducting Pd/Pt layers separated by insulating CoO₂ layers, reflected in a large transport anisotropy ρ_c/ρ_a exceeding 1000. The layered triangular crystal lattice leads to an almost hexagonal Fermi surface (FS)⁴ with little warping, which has been well characterized by de Haas-van Alphen oscillations⁵ and angle-dependent magnetoresistance oscillations⁶⁻⁸. These materials are the most conductive oxides known, with an in-plane mean free path of more than 20 μm at low temperatures^{5,8,9}.

The strong anisotropy is also reflected in the growth of thin plate-like crystals, a common property of layered materials. While mesoscopic quantum phenomena are successfully probed in the plane of quasi 2D ultra-pure metals, achieving such transport perpendicular to the layers is challenging. We have overcome this difficulty by employing focused ion beam (FIB) micro-structuring techniques. Starting from as-grown crystals, we have milled pillars along the c-axis, thereby restricting the in-plane dimensions to few micrometers. A typical structure designed for four-point resistivity measurements is shown in figure 1A. Since the cross section of the pillar is well below the mean free path, the system enters the ballistic transport regime in the plane.

Applying an in-plane magnetic field at low temperatures, we find an oscillatory magnetoresistance (figure 1B). These oscillations are clearly visible in the raw data ($\Delta\rho_{osc}/\rho \sim 5\%$, Figure 1). To perform further

analysis, we focus on the second derivative of the magnetoresistance (figure 1C). The oscillations are periodic in magnetic field, distinguishing them clearly from Shubnikov-de Haas (SdH) oscillations, which are periodic in the inverse magnetic field¹⁰. The oscillation amplitude also does not grow with applied field strength as the Dingle-term of quantum oscillations would. Further, the SdH effect is a sample shape independent property of the Fermi surface, while the here oscillations reported here are dependent on the sample size. The oscillation period varies with the width of the device as it is changed by nearly a factor of three, from 2 μm to 5.5 μm (figure 1D).

The observed periodicity matches remarkably well that expected for a magnetic flux quantum $\Phi_0 = h/e$, with the Planck constant h and electron charge e , threading through an area S enclosed by two adjacent Pd/Pt layers and the sample side walls (dashed line in figure 1D). This gives an area $S = w \cdot c/3$, where w is the width of the sample and c denotes the crystallographic unit cell (PdCoO₂: 1.774 nm; PtCoO₂: 1.781 nm)¹¹. Due to the ABC stacking the unit cell contains three Pd/Pt layers, hence the relevant height is $c/3$. Such oscillations of the magnetoresistance, periodic in Φ_0 as shown by the maxima and minima positions of the oscillations (figure 2A), clearly signal quantum interference in the bulk crystal over remarkable length scales. The sample width is several micrometers, thus indicating that phase information is preserved macroscopically. The observation of phase coherence in a high carrier density metal over such a long distance is surprising and adds a new aspect to the long-range ballistic transport in the plane¹². Yet more noteworthy is the small interlayer distance of only 0.6 nm. On this length scale the atomic orbitals overlap, raising the question of why, and how, the flux in the area S can alter the phase between the nearest layers. However, as this is the case, naively one would expect a quantum process, depending on the flux in an area S , also to lead to processes depending on multiple layers in a stack ($2S, 3S, \dots$). Those multi-harmonic oscillations were demonstrated in quantum hall based interferometers¹³, but are not observed experimentally here, as evidenced by the absence of $h/2e$ oscillations within the noise level of 1% of the h/e oscillations (figure 2B).

So far, we have only considered magnetic fields applied perpendicular to the sample surface. If indeed the oscillation frequency is set by the flux through the area S , it would be natural to expect a sinusoidal dependence on the magnetic field angle, when rotating within the Pd/Pt layer. The oscillation amplitude would at the same time be suppressed due to the superposition of oscillations with different areas S .

The experimental frequency spectrum upon rotation is more complex, with multiple frequencies appearing (figure 3). A natural geometric interpretation of the angle dependence is found within the hexagonal FS of PdCoO₂. The almost perfect hexagonal FS, in contrast to a circular one, exhibits three preferential directions of electron motion perpendicular to the flat faces of the FS. In real space this describes three interleaving subsystems of directional electron flow in the plane, each spanning its own area S_i (sketched in figure 3). The flux enclosed in each subsystem contributes oscillations of frequency $|\vec{B} \cdot \vec{S}_i|/\Phi_0$ to the total conduction, leading to three, 60° offset, branches in the frequency spectrum. The difference in symmetry between the hexagonal FS and the rectangular sample shape divides the branches into two different types. The samples are cut such that one preferential direction of motion is aligned with a sample side wall. Therefore, one subsystem area is set by the full sample depth, while two symmetric branches are related geometrically to the sample width. The aspect ratio of the cross section is reflected in the relative ratio of the maximum frequency values in the two types of branches.

The B -periodic quantum coherent transport observed here is clearly set apart from other magnetoresistance oscillation phenomena such as SdH¹⁰, holographically induced oscillations in 2D electron gases¹⁴ and Bloch-oscillations seen in graphene superlattices¹⁵, as those are periodic in $1/B$. Long range coherence requires macroscopic phase stability which is typically lost due to decoherence at elevated temperatures. This is self-evidenced by the temperature dependence of the SdH oscillations, which describe an interference process in k -space. SdH oscillations are observed in our samples, further demonstrating the high crystal quality of the micro-structures, yet this quantum phenomenon is limited to low temperatures. Given the effective mass of the quasiparticles of $m^* \approx 1.5 m_e$ (PdCoO₂⁵) $1.2 m_e$ (PtCoO₂⁶) the SdH oscillations vanish at 5 K. In contrast, the effect of quantum interference in the out-of-plane transport persists up to much higher temperatures (figure 4). The amplitude is almost temperature independent below 20 K and falls gradually up to 60 K. Naively one might expect the onset temperature

of the oscillations to depend on the sample dimensions, as their observation requires the quantum coherent mean free path, which is strongly temperature dependent, to become larger than the sample width. In contrast, our data shows little difference in the temperature dependence for samples that vary by more than a factor 2 in width (figure 4B), indicating a rather sharp rise in the quantum coherent length scale.

The main focus of this manuscript is to report on this surprising and unexpected magnetoresistance oscillation phenomenon in the interlayer transport. B -linear oscillations, such as semi-classical resonances (Sondheimer¹⁶), interlayer superconducting flux quantization (intrinsic Josephson junctions¹⁷), cyclotron motion in thin films (Azbel-Kaner¹⁸) and interference between parallel quantum wells¹⁹, by themselves, are rare phenomena in single crystals. None of these can explain our magnetoresistance oscillations. Next we discuss and appraise some alternatives, to frame just how unusual the data presented in figures 1-4 are.

At first glance, an explanation of the presented experimental results by the Aharonov-Bohm effect (ABE) may be appealing. However, at the moment we cannot rule out other, more exotic phenomena, such as many-body effects or interference in momentum space²⁰ as suggested in GaAs double layers or Weiss-oscillations in antidot arrays, which can lead to oscillation periodic in B as well as $1/B$ ²¹. Even an Aharonov-Bohm like picture in a bulk crystal, rather than a mesoscopic ring, raises new challenges in the description of electrons in solids.

The initial discovery of the ABE was challenging, as the dominant process is not the ABE akin to the interference in two arms of an interferometer, but rather self-interference due to weak localization, the Al'tshuler-Aronov-Spivak (AAS) effect²². At that time the AAS effect was particularly prominent in the samples, for which the elastic mean free path was much smaller than the sample size. The AAS effect leads to oscillations periodic in $h/2e$, which are always seen to coexist with the ABE oscillations periodic in h/e in metallic rings^{2,3,23}. While the AAS always leads to a maximum in resistance in zero magnetic field, the phase in the ABE is sample dependent. For a structure with multiple rings in series, the AAS effect has experimentally been shown to be independent of the number of rings, while ABE is exponentially suppressed^{24,25}. The layered structure of our samples is reminiscent of a series of rings and our data suggests a maximum in resistance at zero magnetic field for all measured samples (shown in fig2A), similar to AAS. However, it still shows an h/e periodicity of the ABE, while $h/2e$ periodicity of AAS is unobserved. In consequence, neither the simple picture of AAS or ABE completely capture the experimental observations.

A second key feature of our observation is its robustness to temperature. The observation of the ABE in metallic rings was limited to below 1K because of the extreme temperature sensitivity of the quantum coherence length, something that is also a feature of reported ABE experiments on graphene²⁶. This is in stark contrast to the 60K temperature scale observed here in highly metallic PdCoO₂ and PtCoO₂. Similar high-temperature quantum coherence has been seen in bismuth nano-wires²⁷, topological nano-ribbons^{28,29}, quantum dots³⁰, carbon nano-tubes³¹ and $1/B$ superlattice oscillations in graphene¹⁵ but the key to its observation in those nano-scale systems was the small length scales involved. Our devices demonstrate phase coherence over macroscopic length scales of several micrometers (approximately 2×10^4 lattice spacings), and at temperatures of up to 60K.

In an ABE-like scenario, the experimentally observed flux area S would involve an atomic separation between macroscopically extended paths of the interferometer (figure 1A). The interlayer distance of 0.6nm would, to the best of our knowledge, be the smallest linear dimension in any ABE realization. Key to an interferometer are two well-separated paths. Yet interlayer hopping would in principle allow an infinite number of paths and so destroy interference. While the layered structure is reflected in the hopping integral anisotropy, the out of plane value is still significant ($\tau_1 = 1\text{eV}$; $\tau_{zz} = 10\text{meV}$)⁸. This out of plane hopping is consistent with the metallic transport along the c -axis as well as the Fermi surface warping seen by de Haas-van Alphen⁵ effect measurements. The small Fermi wave vector $k_F = 0.1\text{nm}^{-1}$ results in about 8000 periods in each Pd/Pt layer over which the phase information is preserved.

Our finding highlights an aspect of out-of-plane transport in ultra-pure metals on the mesoscale that is, to our knowledge, beyond current understanding. A natural question is why it has not been observed before. The answer is that only recent technological advances have enabled experimental investigations of this regime³². The reduction of w from hundreds of microns to a few microns has revealed the oscillations while keeping the non-oscillatory MR (Fig1B) qualitatively similar to that reported in bulk crystals⁸.

We believe that our observation provides strong motivation for future theoretical efforts in this regime of quantum transport. Even if an explanation in the spirit of the ABE were to survive the issues discussed above, an additional question would be on how the transport at the edge of the sample remains coherent, especially in light of the FIB induced amorphization of the region within 10-20nm on the surface. A scenario worthy of further investigation may involve the recently discovered topological aspects of PdCoO_2 ³³. Further experimental efforts may resolve whether this effect is restricted to the specific case of ultra-pure delafossites or could be a generic property of layered metals. Good test candidates are highly anisotropic materials such as ruthenates, where coherent out-of-plane transport has already been observed similar to PdCoO_2 ³⁴, and in-plane mean free paths can be a micron or longer. Understanding the wave-like nature of electrons in such systems may help to uncover the mechanism that leads from a semi-classical correlated electron system to a macroscopically coherent state such as unconventional superconductivity. Furthermore, how the c -axis coherence evolves upon increasing the number of layers could be approached by fabricating bi- and few-layer thin films. At the same time, such thin films could also be used to explore technological possibilities. Based on our finding, a novel class of electronic solid-state sensors with a lateral spatial resolution for magnetic fields below 1nm could be envisioned. Such quantum sensors may be realized in bilayer thin film structures and would only sense the flux between them. The observation of this striking phase coherent process in a well-studied, single-band metal may prove to be a prime example of unknown phenomena as well as novel functionalities hiding in seemingly well-understood condensed matter systems.

Methodes

Crystal growth. Single crystals of PdCoO_2 were grown in the evacuated quartz ampule with a mixture of PdCl_2 and CoO by the methathetical reaction : $\text{PdCl}_2 + 2\text{CoO} \rightarrow 2\text{PdCoO}_2 + \text{CoCl}_2$ ³⁵. For PtCoO_2 , PtCl_2 and CoO were used correspondingly. The ampule was heated at 1000°C for 12 hours and stayed at 700-800°C for 5-20 days. In order to remove excess CoCl_2 , the resultant product was washed with distilled water and ethanol.

Micro-structuring. Transport lamellae perpendicular to the Pd/Pt layers were cut from as grown high quality single crystals using a FEI G4 Helios dual beam system. The lamellae were cut using gallium ions at 30kV and a current of 47nA for coarse and 21nA for fine milling. These lamellae were transferred from the crystal to a sapphire substrate by hand using a micromanipulator under an optical microscope. The samples were fixed using two-component araldite rapid epoxy. Low ohmic contacts were achieved by argon etching the surface at 200V for 5min before depositing 5nm of titanium and 100nm of gold. The gold film was partially removed in the FIB, exposing the region of interest of the sample, to avoid parasitic resistances. In the final step, the sample is patterned to ensure a homogenous current flow along the c -axis (figure 1A). Three different samples were prepared (two from PtCoO_2 and one from PdCoO_2). After measuring the temperature, field and in-plane angle dependence of all samples, the width of one PtCoO_2 structure was reduced to 2 μm using a Zeiss CrossBeam FIB. All sample dimensions were measured using a scanning electron microscope and are listed in supplementary table 1.

Resistivity Measurements. Resistivity measurements were carried out in a 14T Quantum Design PPMS using a single axis rotator. A SynkTek multichannel lockin-amplifier was used to perform four-point resistance measurements. An alternating current of 100 μA at a frequency of 177Hz was used for the measurements. This was done by sourcing a voltage to the sample in series with a current limiting resistor (1k Ω).

References

1. Davisson, C. J. & Germer, L. H. Reflection of Electrons by a Crystal of Nickel. *Proc. Natl. Acad. Sci. United States Am.* **14**, 317–322 (1928).
2. Chandrasekhar, V., Rooks, M. J., Wind, S. & Prober, D. E. Observation of Aharonov-Bohm electron interference effects with periods h/e and $h/2e$ in individual micron-size, normal-metal rings. *Phys. Rev. Lett.* **55**, 1610–1613 (1985).
3. Webb, R. A., Washburn, S., Umbach, C. P. & Laibowitz, R. B. Observation of the Aharonov-Bohm oscillations in normal-metal rings. *Phys. Rev. Lett.* **54**, 2696–2699 (1985).
4. Noh, H. *et al.* Anisotropic Electric Conductivity of Delafossite PdCoO_2 Studied by Angle-Resolved Photoemission Spectroscopy. **256404**, 1–4 (2009).
5. Hicks, C. W. *et al.* Quantum oscillations and high carrier mobility in the delafossite PdCoO_2 . *Phys. Rev. Lett.* **109**, 1–5 (2012).
6. Kikugawa, N. *et al.* Interplanar coupling-dependent magnetoresistivity in high-purity layered metals. *Nat. Commun.* **7**, 1–8 (2016).
7. Prentice, J. C. A. & Coldea, A. I. Modeling the angle-dependent magnetoresistance oscillations of Fermi surfaces with hexagonal symmetry. *Phys. Rev. B* **93**, 1–11 (2016).
8. Takatsu, H. *et al.* Extremely Large Magnetoresistance in the Nonmagnetic Metal PdCoO_2 . *Phys. Rev. Lett.* **111**, 056601 (2013).
9. Mackenzie, A. P. The properties of ultrapure delafossite metals. *Reports Prog. Phys.* **80**, 032501 (2017).
10. Shoenberg, D. *Magnetic oscillations in metals*. (Cambridge University Press, 1984). doi:10.1017/CBO9780511897870
11. Tanaka, M., Hasegawa, M. & Takei, H. Crystal growth of PdCoO_2 , PtCoO_2 and their solid-solution with delafossite structure. *J. Cryst. Growth* **173**, 440–445 (1997).
12. Bachmann, M. D. *et al.* Super-geometric focusing on the hexagonal Fermi surface of PdCoO_2 . *Arxiv*: 1902.03769
13. Camino, F. E., Zhou, W. & Goldman, V. J. Quantum transport in electron Fabry-Perot interferometers. *Phys. Rev. B* **76**, 155305 (2007).
14. Weiss, D., Klitzing, K. V., Ploog, K. & Weimann, G. Magnetoresistance oscillations in a two-dimensional electron gas induced by a submicrometer periodic potential. *Epl* **8**, 179–184 (1989).
15. Kumar, R. K. *et al.* High-temperature quantum oscillations caused by recurring Bloch states in graphene superlattices. *Science* (80-.). **357**, 181–184 (2017).
16. Sondheimer, E. H. The Influence of a Transverse Magnetic Field on the Conductivity of Thin Metallic Films. *Phys. Rev.* **80**, 401–406 (1950).
17. Ooi, S., Mochiku, T. & Hirata, K. Periodic Oscillations of Josephson-Vortex Flow Resistance in $\text{Bi}_2\text{Sr}_2\text{CaCu}_2\text{O}_{8+y}$. *Phys. Rev. Lett.* **89**, 247002 (2002).
18. Azbel, M. I. & Kaner, E. A. The Theory of cyclotron resonance in metals. *JETP* **30**, 811 (1956).
19. Datta, S. *et al.* Novel interference effects between parallel quantum wells. *Phys. Rev. Lett.* **55**, 2344–2347 (1985).
20. Yakovenko, V. M. & Cooper, B. K. Angular magnetoresistance oscillations in bilayers in tilted magnetic fields. *Phys. E Low-Dimensional Syst. Nanostructures* **34**, 128–131 (2006).
21. Weiss, D. *et al.* Quantized periodic orbits in large antidot arrays. *Phys. Rev. Lett.* **70**, 4118–4121 (1993).

22. Al'tshuler, B. L., Aronov, A. G. & Spivak, B. Z. The Aaronov-Bohm effect in disordered conductors. *P. Zh. Eksp. Teor. Fiz* **33**, 101 (1981).
23. Umbach, C. P., Washburn, S., Laibowitz, R. B. & Webb, R. A. Magnetoresistance of small, quasi-one-dimensional, normal-metal rings and lines. *Phys. Rev. B* **30**, 4048–4051 (1984).
24. Umbach, C. P., Van Haesendonck, C., Laibowitz, R. B., Washburn, S. & Webb, R. A. Direct observation of ensemble averaging of the Aharonov-Bohm effect in normal-metal loops. *Phys. Rev. Lett.* **56**, 386–389 (1986).
25. Beenakker, C. W. J. & Houten, H. Van. Quantum Transport in Semiconductor Nanostructures. **228**, 1–111 (1991).
26. Russo, S. *et al.* Observation of Aharonov-Bohm conductance oscillations in a graphene ring. *Phys. Rev. B* **77**, 085413 (2008).
27. Nikolaeva, A., Gitsu, D., Konopko, L., Graf, M. J. & Huber, T. E. Quantum interference of surface states in bismuth nanowires probed by the Aharonov-Bohm oscillatory behavior of the magnetoresistance. *Phys. Rev. B - Condens. Matter Mater. Phys.* **77**, 17–19 (2008).
28. Peng, H. *et al.* Aharonov-Bohm interference in topological insulator nanoribbons. *Nat. Mater.* **9**, 225–229 (2010).
29. Wang, L. X., Li, C. Z., Yu, D. P. & Liao, Z. M. Aharonov-Bohm oscillations in Dirac semimetal Cd₃As₂ nanowires. *Nat. Commun.* **7**, 1–7 (2016).
30. Sellers, I. R., Whiteside, V. R., Kuskovsky, I. L., Govorov, A. O. & McCombe, B. D. Aharonov-Bohm excitons at elevated temperatures in type-II ZnTe/ZnSe quantum dots. *Phys. Rev. Lett.* **100**, 2–5 (2008).
31. Bachtold, A. *et al.* Aharonov-Bohm oscillations in carbon nanotubes. *Nature* **397**, 673–675 (1999).
32. Moll, P. J. W. Focused Ion Beam Microstructuring of Quantum Matter. *Annu. Rev. Condens. Matter Phys.* **9**, 147–162 (2018).
33. Usui, H. *et al.* Hidden kagome-lattice picture and origin of high conductivity in delafossite PtCoO₂. 1–8 (2018).
34. Ghannadzadeh, S. *et al.* Simultaneous loss of interlayer coherence and long-range magnetism in quasi-two-dimensional PdCrO₂. *Nat. Commun.* **8**, 6–11 (2017).
35. Shannon, R. D., Rogers, D. B. & Prewitt, C. T. Chemistry of noble metal oxides. I. Syntheses and properties of ABO₂ delafossite compounds. *Inorg. Chem.* **10**, 713–718 (1971).
36. Kushwaha, P. *et al.* Nearly free electrons in a 5d delafossite oxide metal. *Sci. Adv.* **1**, e1500692 (2015).
37. Tanaka, M., Hasegawa, M. & Takei, H. Growth and Anisotropic Physical Properties of PdCoO₂ Single Crystals. *J. Phys. Soc. Japan* **65**, 3973–3977 (1996).

Acknowledgements We thank Brad Ramshaw, Ady Stern, Roni Ilan, Mark Fischer, Alberto Mopurgo and Laszlo Forro for helpful discussion. This project was supported by the Max-Planck Society and has received funding from the European Research Council (ERC) under the European Union's Horizon 2020 research and innovation programme (grant agreement No 715730) and the Deutsche Forschungsgemeinschaft (DFG, German Research Foundation) – MO 3077/1-1, as well as the Würzburg-Dresden Cluster of Excellence on Complexity and Topology in Quantum Matter (EXC 2147). M.D.B. and P.M. acknowledges studentship funding from EPSRC under grant no. EP/I007002/1.

Author Contributions C.P., M.D.B., P.M., E.Z, M.K. fabricated the microstructures. Single crystals were grown by S.K. Transport measurements and data analysis were performed by C.P. and P.J.W.M. P.J.W.M., C.P., T.O., R.M. and A.P.M. worked on the interpretation of the data. All authors were involved in the design of the experiment and writing of the manuscript.

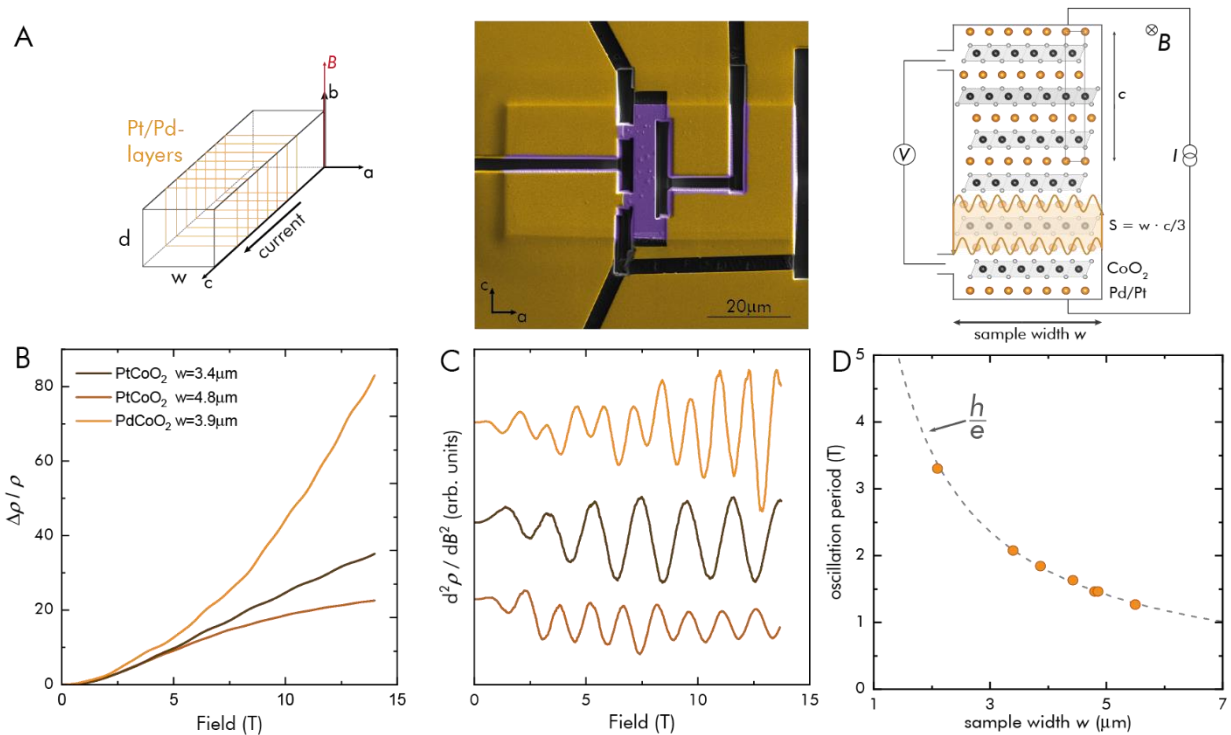


Figure 1: Magnetoresistance oscillations periodic in magnetic field

A) Experimental Setup: (left) Current is passed along a bar shaped sample, perpendicular to the layered structure. The bars have a width w and a thickness d . Magnetic Field is applied and rotated within the Pd/Pt-layer. (middle) SEM image of PdCoO_2 micro structure to measure c -axis resistivity. (right) Crystal structure of PdCoO_2 . Alternating layers of Pd/Pt and CoO_2 layers lead to a high anisotropy of resistivity. The area S relevant for the h/e -oscillations is spanned by two adjacent Pt/Pd layers.

B) Magnetoresistance of PtCoO_2 and PdCoO_2 at $T=2\text{K}$ of various sample widths for fields along the a -axis.

C) The second derivative of resistivity highlights the oscillatory part of the magnetoresistance in panel B.

D) The oscillation period is shown for different sample widths. The sample width dependence shows a remarkable agreement with the oscillation period expected for a single particle magnetic flux quantum, h/e , per area $S = w \cdot c/3$ (as indicated in the panel above).

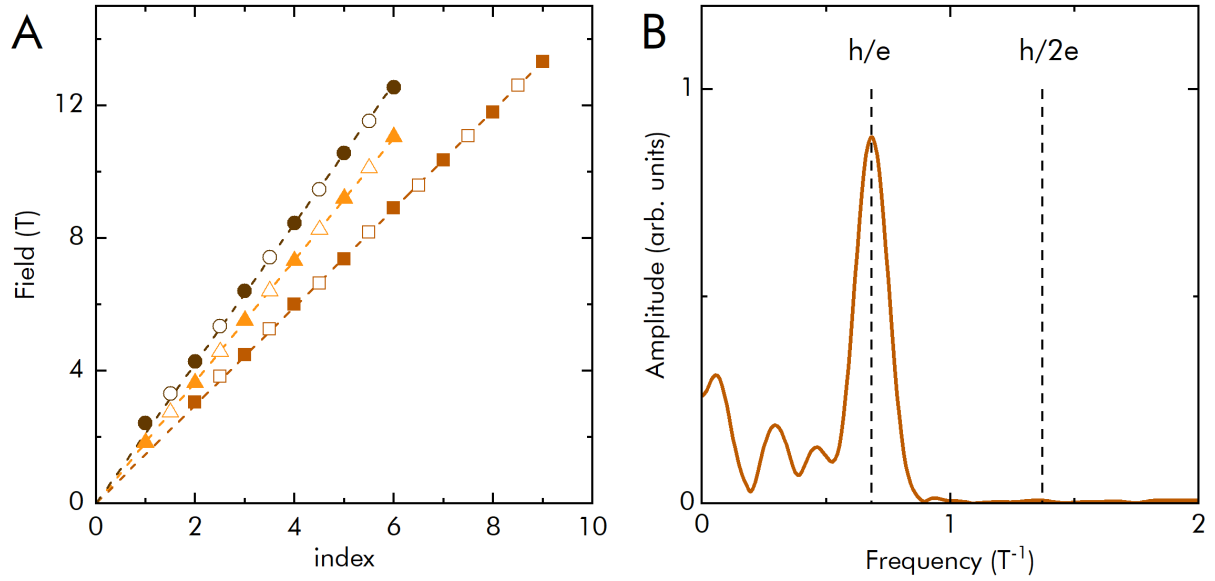


Figure 2: Oscillation period and phase

A) The maxima (solid) and minima (open) positions of the phase coherent oscillations are shown versus the oscillation index for the same samples as in figure 1. (squares - PtCoO₂ 4.8μm; triangles - PdCoO₂ 3.9μm; circles - PtCoO₂ 3.4μm). The dashed line presents a linear in B dependence of the oscillation maxima and minima. The data are in good agreement with the existence of an oscillation maximum in zero magnetic field.

B) Fast Fourier Transform of the data for PtCoO₂ $w=4.8\mu\text{m}$ (dataset shown in Fig 1 C). The dashed lines indicate the frequency positions for the h/e and $h/2e$ oscillations in a box of $S=w*c/3$ as illustrated in Fig 1A. If present, the amplitude of oscillations with period $h/2e$ is a factor 100 times smaller than h/e oscillations, within the experimental noise.

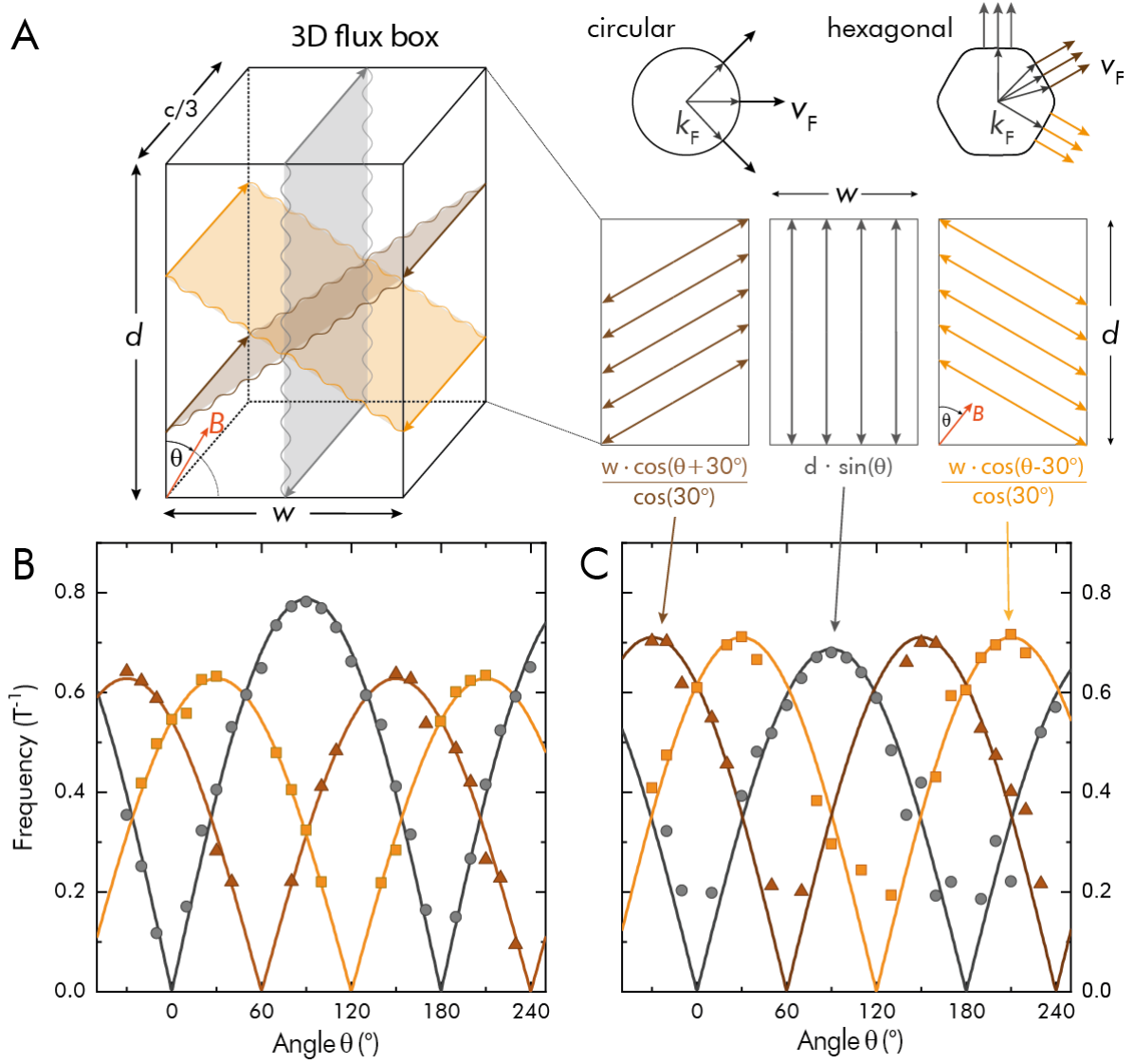


Figure 3: Angle dependence of quantum coherent oscillations.

A) Pd/PtCoO₂ possess almost hexagonal Fermi surfaces^{4,36}. This leads to three preferred directions of motion in contrast to the case of a circular Fermi surface. The magnetic field is rotated in the planes. The three ballistic paths and their angle dependent projections on the magnetic field are shown. In rectangular samples two symmetric branches are set by the sample width and one by the sample thickness d . The left panel illustrates the relevant 3D flux box limited by the sample width, thickness and two adjacent Pd/Pt-layers. This box defines the flux surfaces. The oscillations are periodic in integer flux quanta threading through them.

B+C) Angle dependence of the quantum coherent oscillations of PdCoO₂ (B) and PtCoO₂ (C). Solid symbols represent the measured data points, solid lines show the expectation from the model sketched in panel A. B) shows data from a sample with a d/w -ratio of 0.7, while the ratio for the sample in panel C is close to 0.9.

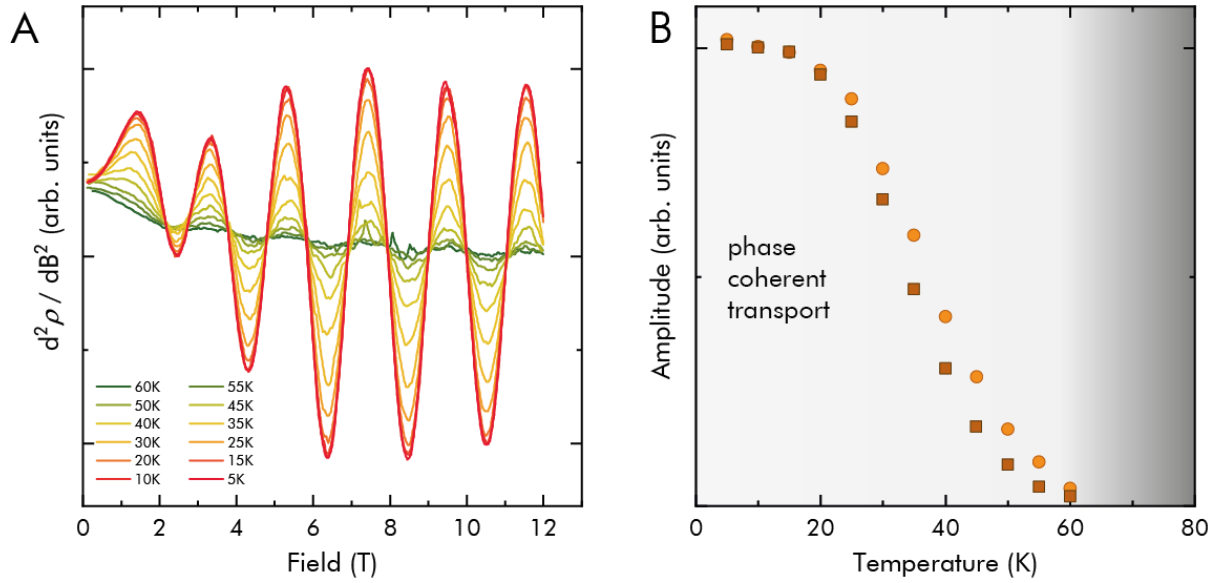


Figure 4: Temperature dependence of the phase coherent oscillation amplitude.

A) Second derivative of the magnetoresistance of PtCoO₂ ($w = 4.8\mu\text{m}$). Oscillations persist up to 60K.

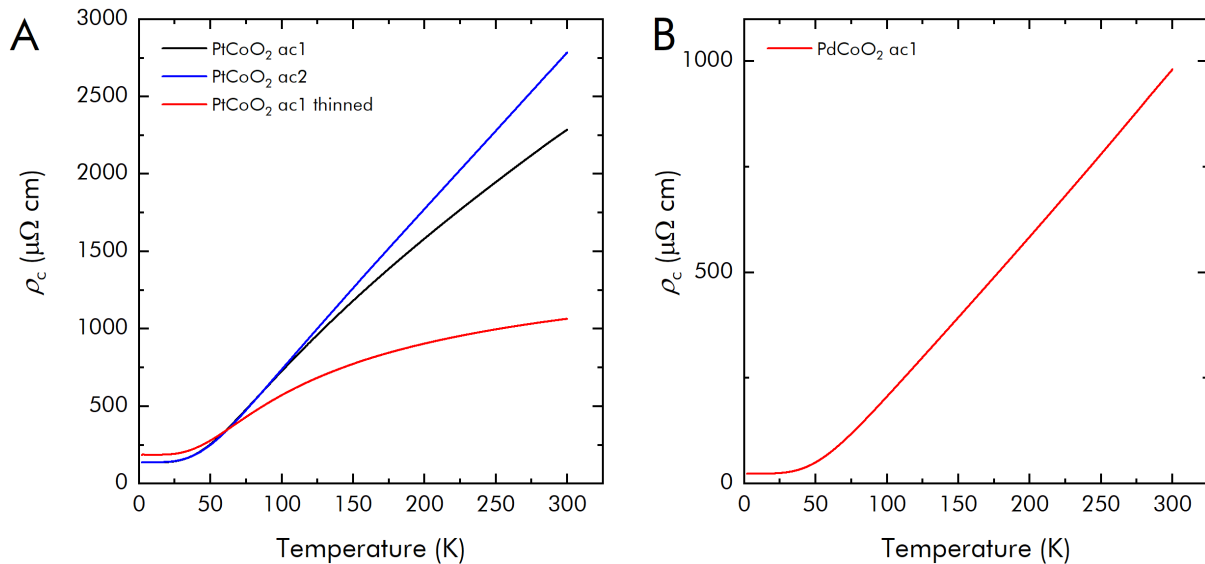
B) Oscillation amplitudes extracted from Fast Fourier Transform analysis in the field range from 3T to 12T are shown for PtCoO₂ $w = 4.8\mu\text{m}$ (squares) and $w = 2.0\mu\text{m}$ (circles). The phase coherent oscillations show little temperature dependence below 20K before a gradual decrease to 60K. This demonstrates the strong resilience of the quantum phase coherence to temperature. The onset temperature of approximately 60K has little dependence of sample width.

Supplementary Information

Supplementary Table 1: Sample information

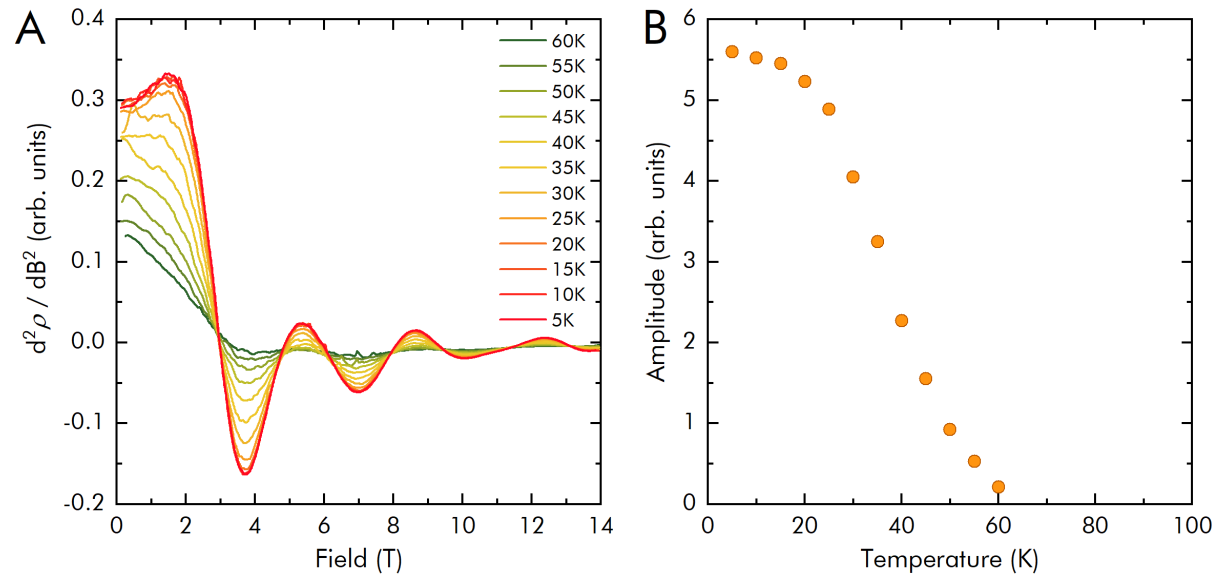
Sample	w (μm)	d (μm)	l (μm)	$\rho(2\text{K})$ ($\mu\Omega\text{cm}$)	$\rho(300\text{K})$ ($\mu\Omega\text{cm}$)
PtCoO ₂ ac1	4.76	4.5	14.7	136	2284
PtCoO ₂ ac1 thinned	2.0	4.5	14.7	186	1064
PtCoO ₂ ac2	3.4	4.8	19.5	138	2784
PdCoO ₂ ac1	5.5	3.9	22.3	23	979

Supplementary Figure 1: Zero field cool of resistivity.



Resistivity as a function of temperature for the samples use in this study. A metallic behaviour is found for the c-axis resistivity for all devices. The data are in good agreement with previous reports on bulk single crystals³⁷. A strong dependence on the smallest in-plane sample dimension is observed. In the high temperature limit the behaviour would be consistent with a parallel conduction path that does not scale with the sample cross-section but rather its circumference. This contrasts with the low temperature limit where an increase in the resistivity is observed suggesting that this surface layer, if it exists, becomes strongly insulating while also taking up 25% of the sample cross section. An amorphous surface layer caused by FIB is usually on the length scale of 10nm and would hence not explain this situation³².

Supplementary Figure 2: Temperature dependence PtCoO₂ thinned

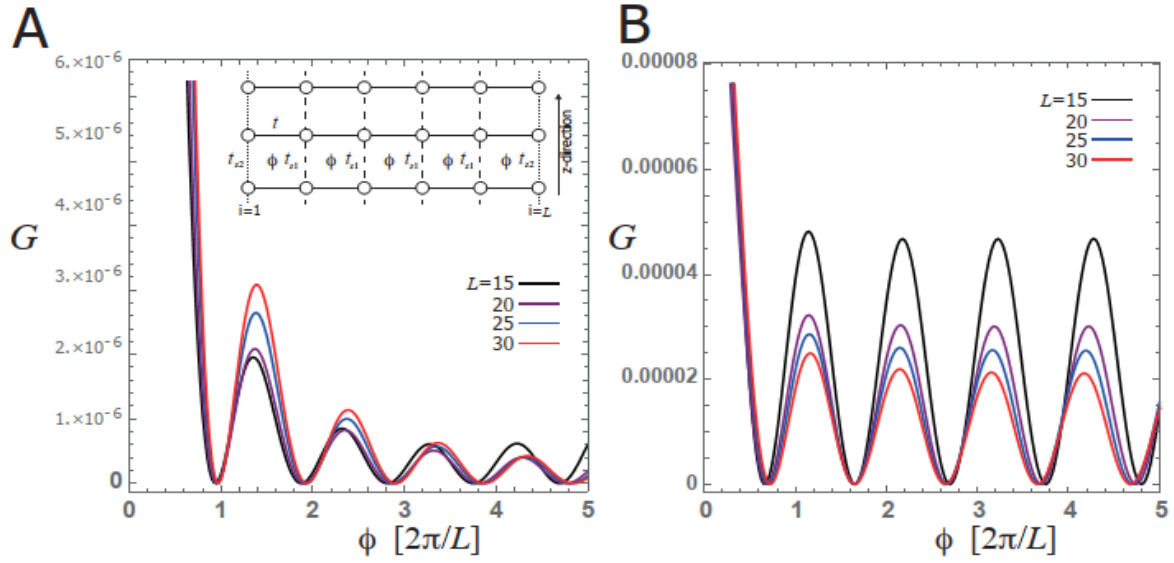


Supporting data for Figure 4 of the main manuscript.

A) Second derivative of magnetoresistance with respect to magnetic field for PtCoO₂ $w=2\mu\text{m}$.

B) Temperature dependence of the oscillation amplitude of the data shown in panel A. The data are identical to that shown in figure 3B.

Supplementary Figure 3: Calculated inter-layer conductance



Calculated inter-layer conductance as a function of magnetic flux piercing a layered lattice system. Inset of A shows the details of the model. One dimensional tight binding chains with hopping t models the transport within the Pt layers, while the interlayer hopping is described by the small hopping parameter t_{z1} (set to $0.001 t$). At the edge, we allow an enhancement in the interlayer hopping t_{z2} to examine the effect of a possible metallic surface layer formed by FIB (A: $t_{z2} = t_{z1}$ without surface layer, B: $t_{z2} = 5 t_{z1}$ with surface layer). The conductance is calculated from the intra-band Kubo formula. The results show an oscillation with the periodicity $\Delta\phi = 2\pi/L$, which translates to the h/e oscillation in the box of size $S = w^*c/3$. The oscillation is largely enhanced if we assume that a metallic surface layer is formed by FIB (B). However, this contribution reduces as $1/L$ and may not explain the measured oscillation. For the measured samples $L \approx 8000$ and varies by more than a factor 2 without significant change in oscillation amplitude.

The intra-band Kubo formula is given by $G_{intra-band} = \left(\frac{ie^2}{\omega + i\eta} \right) \left[\frac{1}{V} \sum_{k,n} \left(-\frac{\partial f}{\partial \varepsilon_{kn}} \right) v_{knz} v_{knz} \right]$, where ε_{kn} is the eigenenergy, k is the z-momentum, $n=1, \dots, L$ the eigenstate index, f the Fermi distribution, v_{knz} the expectation value of the z-current operator, and the frequency ω is set to zero, where η is a small relaxation parameter.

Note: We don't divide by L so G is a conductance and not a conductivity.